

Structural evolution in high-pressure amorphous CO₂ from *ab initio* molecular dynamics

Dušan Plašienka* and Roman Martoňák

Department of Experimental Physics, Comenius University,
Mlynská Dolina F2, 842 48 Bratislava, Slovakia

(Dated: October 29, 2018)

By employing *ab initio* molecular dynamics simulations at constant pressure we investigated behavior of amorphous carbon dioxide between 0-100 GPa and 200-500 K. We focused on evolution of the high-pressure polymeric amorphous form known as a-carbonia on its way down to zero pressure, where it eventually converts into a molecular state. During the simulations we observed a spectrum of amorphous forms between two limiting polymeric forms with different proportion of three and four-coordinated carbon atoms. Besides that we also found a new mixed molecular-polymeric form that shows pronounced metastability at certain conditions. The observed behavior suggests CO₂ as possible candidate for polyamorphism. We discuss structural and physical properties of the observed amorphous forms as well as their relations to crystalline phases.

PACS numbers: 61.43.Bn, 61.43.Dq, 64.70.K-, 81.30.Hd

I. INTRODUCTION

Pressure-induced amorphization (PIA) and amorphous-amorphous transition (AAT), as well as liquid-liquid transition (LLT), are fundamentally interesting and widely studied phenomena occurring in some common materials¹⁻³. Especially interesting is the existence of polyamorphism, both in the solid regime - AAT, as observed in H₂O, SiO₂, GeO₂⁴⁻⁷, Si⁸, Ge⁹, S¹⁰ or C¹¹ and in the liquid state - LLT, as reported experimentally in P¹² and S¹³ (and disputed in N¹⁴⁻¹⁶) or predicted theoretically for C¹⁷ and H¹⁸. Recently, carbon dioxide has been found to enrich this class of materials for observing the AAT between extended a-carbonia and molecular amorphous forms^{19,20} and also for prediction of LLT between molecular and polymeric liquids^{21,22}.

Carbon dioxide is one of the most important compounds found on Earth and in the Solar system, which plays a crucial role in planetary atmospheres and influences also dynamics of their interiors. At the same time, crystallography and high-pressure behavior of CO₂ are nontrivial and attracted a lot of attention in the last 15 years leaving some topics still unresolved (see reviews²³⁻²⁵). The exact structure of (pseudo-sixfold) phase-VI (see Refs.²⁶⁻³⁰), intermediate character and possible presence of bent molecules in phases II, IV and III - see^{20,31-41}, for example, are still matter of debate. The high-*P-T* regime of CO₂ is also disputed as far as several experiments and theoretical works often led to conflicting results^{21,22,42-48}. A liquid-liquid-solid triple point was recently proposed to exist inside the Earth's geotherm region as well^{21,22}.

The lowest pressure solid molecular phase of CO₂, present on surface of icy caps of Mars, is known as dry ice - phase-I. This quadrupolar *Pa3* structure transforms between 12-18 GPa into *Cmca* phase-III^{31,49,50} with molecules aligned in planes, which on further compression transforms into tetrahedral phase-V^{31,51}, recently

identified as β -cristobalite *I42d* structure^{52,53} (though existence of a tridymite-like *P2₁2₁2₁* structure at similar conditions is was also proposed⁵⁴). Other stable phases of CO₂ include molecular phases II³³, IV^{34,36} and VII⁵⁵, polymeric phase-VI²⁶ and other newly discovered forms - possibly polymeric phase-VIII⁵⁶, two tetrahedral structures of coesite-I (phase-IXa) and coesite-II (phase-IXb)⁵⁷ and ionic phase *i*-CO₂⁴⁷.

A specific property of phase-V (and all tetrahedral structures of CO₂) is extreme rigidity of intertetrahedral C-O-C angle that is represented by energy calculations of *I42d* phase⁵⁸ and H₆C₂O₇ molecule⁴³, which both show a dramatic increase in energy with variation of the angle out of deep minimum placed near 125°. This behavior is in a sharp contrast with SiO₂, where the minimum is shallow and allows silica to form a rich variety of *sp*³-polymorphs⁵⁸ unlike the situation in CO₂. High stability of tetrahedral over possible octahedral structures in CO₂ is also obvious and might be connected to small size of carbon atoms that allow them to occupy interstitial sites of the close-packed oxygen sublattice²⁸. Stiff C-O-C angle is directly connected also to low compressibility of tetrahedral CO₂.

As far as double C=O bond is one of the most stable chemical bonds, molecules sustain large overpressurization before they break and initiate transformation into a single-bonded network. Molecular phase-III hence persists to (60 GPa, 300 K) and to (40 GPa, 1800 K)³¹, though the equilibrium transition pressure is according to recent experiment⁵⁹ and enthalpy calculations^{30,42,43} only around 20 GPa. The molecular-to-nonmolecular transition is therefore associated with high free energy barriers that lead to negative slope of (kinetic) transition line⁶⁰ and possibly also to amorphization at low and moderate temperatures when system is not able to complete the transition and remains stuck in a disordered state.

SiO₂ and GeO₂ are archetypal glass-forming materials exhibiting low and high density tetrahedral amorphous

forms (LDA and HDA) as well as octahedral forms and forms containing fivefold coordinations⁴⁻⁷. The first prediction of tetrahedra-based amorphous CO₂ was based on *ab initio* molecular dynamics (MD) simulations in the work of Serra *et al.*⁶¹ in 1999 and the first observation of amorphous CO₂ was reported two years later³⁴. It was suggested from the Raman spectra that the extended amorphous solid is formed by a mixture of three-coordinated (3c) and four-coordinated (4c) carbon atoms³⁴, which would be a novel property amongst the group-IV dioxides. Synthesis of a-CO₂ was also reported in Ref.⁶² and in the further experiments, Santoro *et al.*¹⁹ suggested from Raman spectra that amorphous polymeric form of CO₂, named "a-carbonia", is a glassy counterpart of phase-V and is also similar to tetrahedral a-silica. Another experimental study was performed at room temperature by Kume *et al.*²⁰ and a-carbonia was proposed to be related to phase-VI. In these experiments, a-carbonia was decompressed to ambient conditions and a transformation into a molecular amorphous form was observed - at 16 GPa¹⁹ and below 30 GPa²⁰. Amorphization in the higher *P* region was observed on further compression of phases V, VI and coesite-CO₂ over 1 Mbar⁴⁷.

Amorphous CO₂ was studied also by first principles simulations (MD²⁷ and metadynamics²⁹), which confirmed the picture of mixed three and fourfold nature of a-carbonia, while in both references roughly equal number of 3c and 4c atoms was reported. Recent *ab initio* calculations proposed also existence of a first-order LLT between molecular and polymeric liquids^{21,22} - the polymeric liquid is formed from the molecular one starting as predominantly 3c but evolves upon compression to 4c-dominated liquid form.

The experimental and theoretical works leave several questions about amorphous carbon dioxide open. In particular, what is the actual structure of a-carbonia - what is the stable ratio of 3c and 4c carbons (3-4 ratio) at different pressures and what is the structural relation between a-carbonia and crystalline CO₂. Furthermore, how the structural evolution from a-carbonia to the molecular amorphous form proceeds and what exactly happens upon (de)compression - if the transformations are continuous or discontinuous and whether molecules can eventually coexist with the polymeric form. In this paper, we aim at resolving these questions using *ab initio* MD.

The paper is organized as follows. In part II, we describe methods and main findings of our simulations that are analyzed in part III. The analysis includes investigation of structural properties of polymeric amorphous forms and mixed molecular-polymeric form and their possible relations to crystalline phases. Next, mechanical stability of the observed forms is analyzed and compared. Finally, enthalpies, compressibilities, electronic properties and structure factors of all forms are calculated and discussed. Finally, we summarize our observations and suggestions for further study in the conclusions.

II. SIMULATION METHODS AND PROTOCOL

We used standard density functional theory (DFT) based codes VASP 4 and 5^{63,64}. To simulate systems under constant pressure with VASP 4 version, we employed slightly modified Berendsen algorithm⁶⁵ where cell parameters and atomic positions and velocities were rescaled according to difference of external and internal stress tensor every 20 MD timesteps (more details are described in Ref.⁶⁶). Simulations performed with newer versions of VASP 5 were carried out with the implemented Parrinello-Rahman (PR) barostat⁶⁷ working together with the Langevin thermostat generating the *NPT* ensemble. PAW pseudopotentials and the PBE functional⁶⁸ were used to describe four/six valence electrons for each carbon/oxygen atom, using energy cutoff 450 eV and Γ -point sampling of the Brillouin zone.

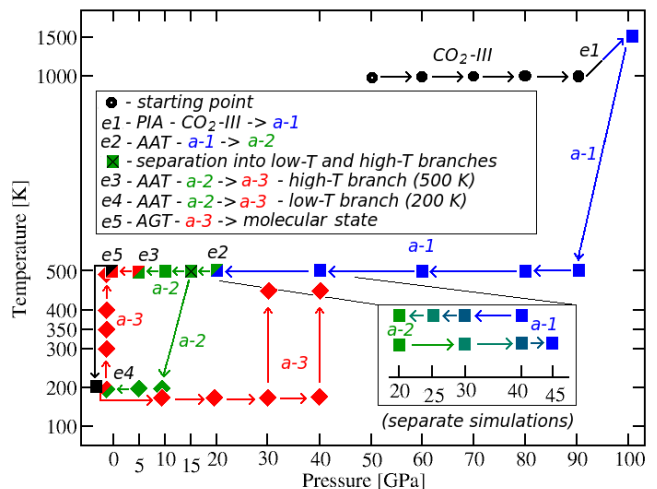


FIG. 1: (Color online) Simulation protocol of solid CO₂. Starting from phase-III (black dots and arrows) at 50 GPa and 1000 K, PIA was observed at 100 GPa - event-1 (e1) leading to formation of polymeric a-carbonia form denoted as *a-1* (blue squares and arrows). Decompression at 500 K led to creation of another version of polymeric a-carbonia *a-2* (green squares) - event-2 (e2) and on further pressure drop *a-3* (red squares) was formed at 5 GPa - event e3. The same *a-3* form (red diamonds) was created independently at 0 GPa and 200 K - e4. In the 500 K simulation branch, molecular state (black) appeared at 0 GPa - e5. In the inset are shown separate simulations of compression of *a-2* and decompression of *a-1* between 20 and 45 GPa at 500 K performed in more pressure steps and for longer times as in the original simulation. The turquoise color of the squares represents forms with intermediate character between blue *a-1* and green *a-2*.

We ran all simulations on fairly large systems consisting of 108 CO₂ molecules. After optimization of phase-III (black) to 50 GPa, we started dynamical simulations by heating the system to 1000 K and then increasing pressure in 10 GPa steps (Fig. 1). Sample amorphized upon compression from (90 GPa, 1000 K) to (100 GPa, 1500 K) similarly to previous DFT simulations⁶¹. The result-

ing polymeric *a*-carbonia form (blue), which we denote as *a-1* here, was dominated by 4c carbons (CO_4 tetrahedras). From this point, we started decompression at temperature of 500 K in order to study the evolution of the amorphous state. After bringing system to 20 GPa, *a-1* was transformed to a different polymeric form with similar proportion of 3c and 4c carbons - *a-2* (green). Amorphous forms *a-1* and *a-2* appear in our simulations as two limiting (high and low pressure) realizations of polymeric *a*-carbonia because they transform into each other gradually between 20 and 45 GPa as observed in separate calculations shown in the Fig. 1 inset.

Afterwards, we proceeded with decompression along two separate pathways - at 500 K and at 200 K⁷⁸. In the 500 K branch we observed a formation of mixed molecular-polymeric form - *a-3* (red) at 5 GPa, while the same form appeared also in the lower 200 K branch at 0 GPa. The two independent kinetic pathways leading to the same amorphous form - with equal proportion of coordinations, suggest that *a-3* form is not a mere artifact of the simulation timescale, but instead a form with pronounced metastability. This is further supported by stability of *a-3* form obtained at (0 GPa, 200 K) on its subsequent compression to 40 GPa and 500 K (see Fig. 1). In the 500 K branch, *a-3* completely depolymerized into a molecular state (black), which behaved like gas at the simulation temperature of 500 K (therefore denoted as amorphous-gaseous transition - AGT on Fig. 1) and solidified to molecular amorphous form at 200 K. The total simulation time of our 324 atomic system exceeds 1 ns.

III. RESULTS AND DISCUSSION

To characterize the various amorphous forms, we analyzed proportion of different carbon coordinations. On Fig. 2, we show the entire run of initial compression and 500 K branch decompression from Fig. 1 spanning total simulation time of 208 ps, where all amorphous states were observed. The amount of carbon two (CO_2 molecules), three and four coordinations are shown in red, green and blue, respectively.

Compression from 90 to 100 GPa (starting at 52 ps) caused immediate breakdown of all molecules and formation of fully-extended disordered network - *a-1*, with 88% of 4c carbons and remaining 12% of 3c atoms. The form *a-1* persisted unchanged on decompression to 40 GPa, but at 20 GPa (at 100 ps) a number of bonds desaturated and a new mixed 3c (40%) and 4c (55%) form - *a-2* containing also 5% of molecules appeared. During simulations at 5 GPa, this form transformed into *a-3* (at about 155 ps) consisting of 18% of 4c carbons, 60% of 3c carbons and 22% of molecules (the same as in the lower 200 K branch, not shown here). At 0 GPa and 500 K, *a-3* finally started to decay (at 185 ps) and all molecules were recovered shortly after (at 199 ps).

Separate simulations of compression of *a-2* from 10 to 45 GPa and decompression of *a-1* from 40 to 20 GPa at

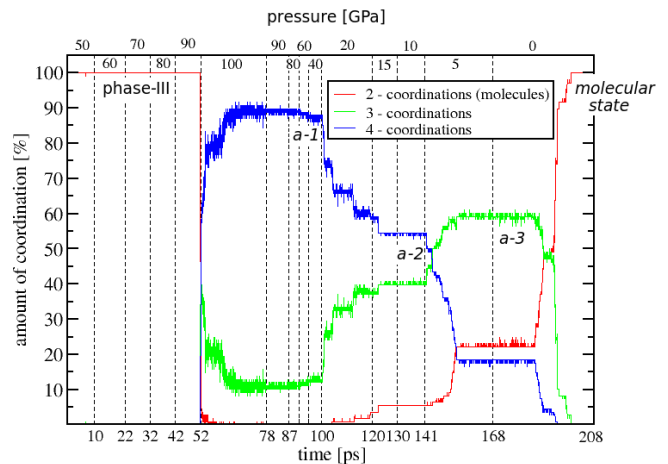


FIG. 2: (Color online) Amount of carbon coordinations [%] on compression (to 78 ps), where *a-1* was formed, and on higher-*T* branch (500 K) decompression (from 78 ps to 208 ps), where all other forms appeared. The CO_2 molecules are shown in red (starting and ending at 100%), 3c are in green and 4c in blue (4c-curve is systematically larger than 3c-curve from 52 to 144 ps and lower thereafter). The coordination limit was 1.7 Å. Vertical dashed lines divide graph into regions of different simulation pressures that are labeled on top and are changed at corresponding times labeled at bottom.

500 K (see inset of Fig. 1) revealed that both forms gradually transform into each other in this pressure window, which can be viewed as a continuous transformation between the two limiting states of amorphous *a*-carbonia - the high-pressure tetrahedral form *a-1* and the low-pressure form *a-2*. The forms are limiting forms of polymeric *a*-carbonia in the sense that further compression of *a-1* does not induce further structural transformation (bonds are saturated) and decompression of *a-2* leads directly into a different amorphous regime represented by the mixed molecular-polymeric form *a-3* (and not to a different polymeric state).

A. Structure of nonmolecular *a*-carbonia

Amorphization occurs very fast upon the compression to 100 GPa and is accompanied by a large volume collapse and complete structural reorganization. From the distribution of intramolecular $\text{O}=\text{C}=\text{O}$ angles, we observed that molecules always remained linear lacking any systematic bending before the onset of amorphization.

Structure of *a-1* form is shown on Fig. 3(a), where a nanocrystallite⁷⁹ of phase-V seems to be formed inside the amorphous network. This points to a structural correspondence between tetrahedral-like form of *a*-carbonia - *a-1* and crystalline phase-V. To prove their relation, short-range order of both forms was investigated and depicted onto Fig. 4. Radial distribution functions (RDFs) - upper panel and angular distribution functions (ADFs) - lower panel of *a-1* and phase-V are shown along each

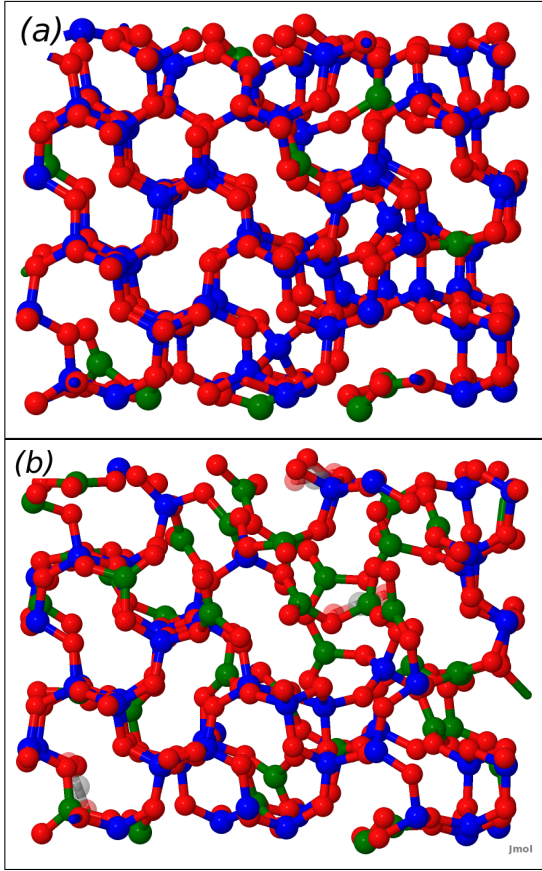


FIG. 3: (Color online) (a) Snapshot of *a-1* at 40 GPa and (b) of *a-2* at 20 GPa and 500 K. 4c and 3c carbon atoms are marked as blue and green spheres, respectively. Pictures were generated by Jmol⁶⁹.

other, while all distribution peaks of *a-1* are broad and for phase-V are sharp. One can see from the figures clearly that all broad peaks of *a-1* well cover the corresponding sharp peaks of phase-V. Regarding the nearest neighbors, value of the C-C coordination number N_C^{CC} of *a-1* is 3.83 at cutoff 2.6 Å and $N_C^{OO} = 11.87$ at 2.7 Å. The C→O coordination $N_C^{C\rightarrow O} = 3.88$ and the O→C coordination $N_O^{O\rightarrow C} = 1.94$ at cutoff 1.7 Å. The corresponding coordination numbers for phase-V are similar - 4, 12, 4 and 2, respectively at the same cutoff values. The *a-1* form can be therefore regarded as an amorphous version of phase-V, as was suggested for experimentally observed a-carbonia from its Raman spectra¹⁹.

An important property of phase-V is rigidity of the intertetrahedral C-O-C angle. The peak of the C-O-C ADF in *a-1* is placed around 118° - Fig. 4 lower panel turquoise curve. This is in a good agreement with the calculated ideal value - 125-130°⁵⁸ or 124°⁴³) and also with the measured angle - 113.2°⁵². The distribution is, however, quite sharp for an amorphous solid (compare e.g. with the wide Ge-O-Ge distribution in a-germania⁷⁰) and indicates that stiffness of the C-O-C angle is a basic property of CO₂ that is inherited into the amorphous

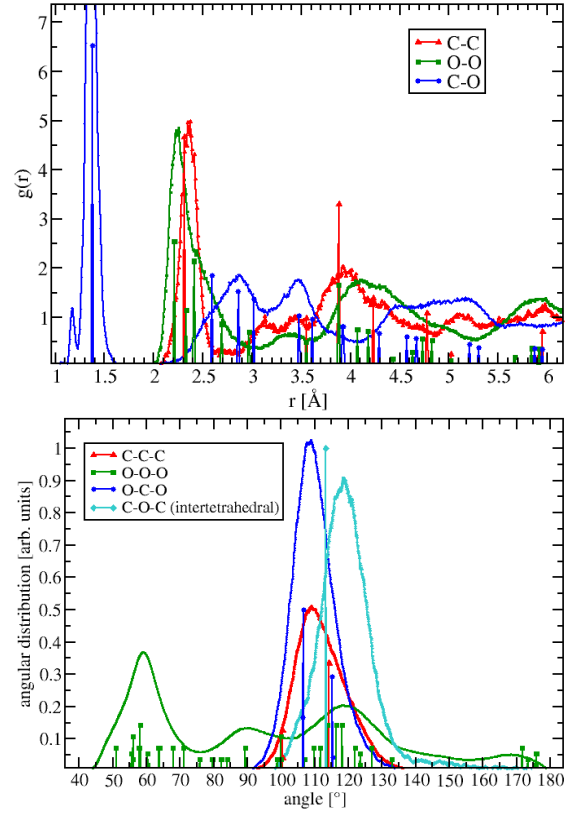


FIG. 4: (Color online) (Upper panel) RDFs of type C-C (red triangles), O-O (green squares) and C-O (blue circles) for *a-1* (broad peaks) at 40 GPa, 500 K and zero- T structure of phase-V at 41 GPa from data provided by Datchi *et al.*⁵² (sharp peaks). The tiny first C-O peak represents C=O bonds from small number of 3c carbons. (Lower panel) ADFs of type C-C-C (red triangles), O-O-O (green squares), O-C-O (blue circles) and intertetrahedral C-O-C (turquoise diamonds) - all calculated within the first RDF minima of *a-1*.

regime.

Similar amorphous form as is our predominantly tetrahedral *a-1* was reported in the previous MD simulations⁶¹. In the original study, it was described as a tetrahedral amorphous solid, while in the subsequent work²⁷, it was stated that it contained unspecified number of unsaturated bonds (we remind *a-1* also contains 12% of 3c carbons). A glass with similar structure was obtained by quenching from 4c-dominated liquid state²².

The second limiting a-carbonia form *a-2* - Fig. 3(b) contains only slightly higher number of 4c than 3c carbons. Very similar forms like this were obtained in the previous *ab initio* simulations, which were performed along different P - T pathways^{27,29}. Direct experimental evidence about the quantities of carbon coordinations (as determined e.g. for amorphous GeO₂⁷) is as yet not available.

B. Structure of molecular-polymeric form

At two different P - T points (e3 and e4 on Fig. 1), the a -2 form independently transformed into substantially different molecular-polymeric amorphous state a -3 shown on Fig. 5(a). To our knowledge this form of a -CO₂ was not discussed so far. The a -3 form represents a mechanically stable local packing of CO₂, CO₃ and CO₄ units forming a bridge between molecular and polymeric amorphous states. The form is composed of three basic units - sp^3 -tetrahedras CO₄, triangles CO₃ and linear molecules CO₂⁸⁰. The molecules remain isolated, while 3c and 4c carbons connect and form several structural patterns. The most abundant are polymeric chains formed by series of 3c carbons pinned to two different 4c carbons (nodes), which are present in various lengths and torsions. Next, we observe closed chains beginning and ending in the same 4c carbon and occasionally also entirely three-coordinated loops (cyclic molecules) shown on Fig. 5(b) and (c). Some of the cyclic (CO₂)_x oligomers were already studied by methods of theoretical chemistry^{71,72}.

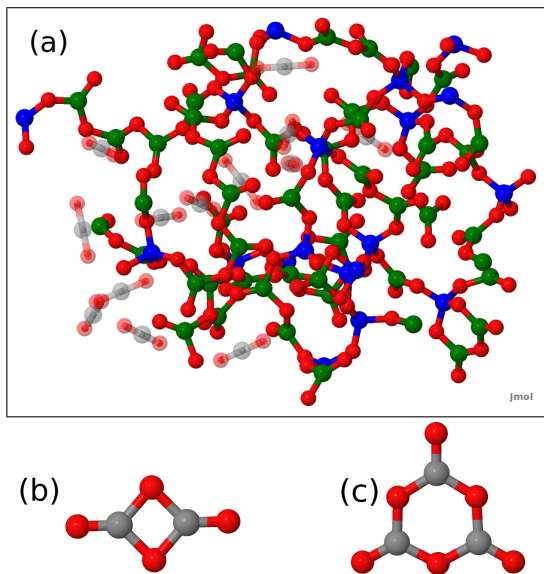


FIG. 5: (Color online) (a) Amorphous form a -3 at 5 GPa and 500 K. One closed chain of two 3c atoms pinned to one 4c carbon is placed near the down right edge of the picture. 4c and 3c carbons are distinguished as blue and green atoms, isolated CO₂ molecules are marked translucent. (b) C₂O₄ dimer and (c) C₃O₆ trimer occurring in the a -3 form.

Formation of C₂O₄ dimeric molecules were observed in MD of high- T liquid phases^{22,73}. In Ref.⁷³, for example, metastability of dimers, which we indeed observe in a -3, was proposed to take place at low temperature. Moreover, it was also suggested that existence of these dimers may represent a kinetic intermediate step on the transformation to some three-coordinated crystalline phase, which is discussed in the next paragraph. In another

theoretical calculations of liquid CO₂, presence of unstable CO₂ molecules in predominantly polymeric liquid form near the proposed LLT line region²² was also observed. This indicates that mechanically stable mixture of molecular and nonmolecular state at low temperatures (in solid state), where the kinetics is considerably slower, may be possible.

We now briefly discuss possible thermodynamical background of amorphous forms containing 3c carbons. Presence of these 3c carbon atoms in a -carbonia and also in form a -3 opens a natural question whether 3c atoms can form some stable or at least metastable structure. While no such phase has been observed experimentally, some theoretical hints exist^{27,72,73}. In our case, fact that a -3 contains chains of 3c atoms as basic building blocks points to the possible relation to a hypothetical crystalline phase composed of infinite parallel chains of 3c carbon atoms. Possibility of such chain forms has been proposed in some previous studies^{27,72,73}.

The initial guess in our search for the 3c form was inspired by Ref.²⁷ and picture of the structure depicted on Fig. 4(b) therein. Following optimizations at several pressures, we found a structure denoted as phase-3C, which is formed by linear zig-zag chains aligned in mutually shifted planes (Fig. 6). Phase-3C has lower enthalpy than molecular phases at pressures over 40 GPa (see Fig. 8). Phase-3C was stable in dynamical simulations at 0 GPa and 200 K for several tens of picoseconds.

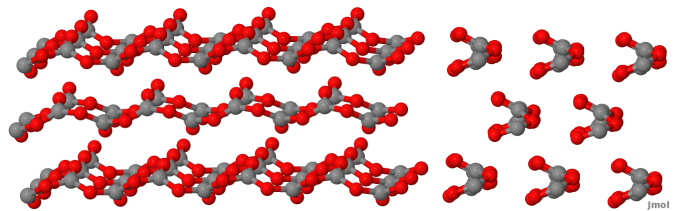


FIG. 6: (Color online) Phase-3C at 10 GPa - front view (left) and chain axis direction side view (right).

C. Structural stability

We turn now to discussion of the behavior of the observed amorphous forms upon change of pressure, namely gradual transformation between limiting polymeric forms a -1 and a -2 and pronounced metastability of the molecular-polymeric a -3 form. To relate the stability upon compression to the network structure we analyze the distribution of nearest distances between possible reaction sites, namely 3c carbons and single-coordinated (1c) oxygen atoms (with double bonds). The distribution of the nearest distances at certain conditions thus reflects the potential ability to turn 3c carbons into 4c ones upon compression. The respective histograms are shown in Fig. 7(a) where we compare at 10 GPa a -3 and a -2 and at 30 GPa a -3 and intermediate state between

a-1 and *a-2* (containing 63% of 4c carbons). At both pressures of 10 GPa and 30 GPa, histograms of *a-3* are shifted away from the corresponding polymeric ones indicating that less possible reaction sites of 3c \rightarrow 4c C transitions are available. Moreover, at 30 GPa, the *a-1/a-2* state contains sizable amount of nearest 3c-C-to-1c-O distances between 1.7 and 2 Å, which allows for gradual evolution of coordinations in the polymeric regime between the limiting forms *a-1* and *a-2*.

The structural stability of the system during decompression, on the other hand, can be related to the relative number of most strained single C-O bonds which are prone to break during the volume increase. To this end we count the fraction of elongated single bonds in the length interval from 1.4 to 1.7 Å - Fig. 7(b). It can be clearly seen that the *a-3* form compared to polymeric forms contains lower amount of elongated single bonds and thus is more stable also with respect to decompression.

D. Thermodynamical, mechanical, electronic and structural properties

To analyze relative zero- T stability of the discussed amorphous and crystalline forms, we calculated equations of states for volume and enthalpy versus pressure - Fig. 8(a) and (b), respectively. Our calculated enthalpy functions show that phase-V becomes more stable than phase-III over 17.5 GPa and molecular phase-I crosses phase-III curve at around 20 GPa, similarly to Ref.³⁹. The three-coordinated Phase-3C (stable up to 60 GPa) is favored over phase-V below 8 GPa and over phase-III above 40 GPa, though it is metastable at all pressures.

Regarding the amorphous forms, *a-1* curve systematically copies curve of the crystalline phase-V with about 0.7 eV higher enthalpy values. The *a-2* form survived optimization only between 10 and 20 GPa, while *a-1* decayed below 30 GPa. This nonstability of both limiting polymeric forms between 20 and 30 GPa observed in the optimization process is related to the existence of the pressure window, where intermediate states between *a-1* and *a-2* were observed in the MD simulations (see inset of Fig. 1). Form *a-3* was stable between 0 and 50 GPa and its enthalpy shows that is more stable than phase-V below 8.5 GPa. This analysis shows that in certain pressure intervals, the amorphous forms have lower enthalpies compared to some competing crystalline phases and might synthesize at carefully chosen experimental P - T conditions.

To calculate bulk moduli of the investigated forms, we run simulations with the Parrinello-Rahman barostat to obtain volume fluctuations $\langle \delta V^2 \rangle$ for NPT ensemble. These fluctuations are proportional to the isothermal bulk modulus B according to the fluctuation formula⁷⁴

$$B = \frac{kT}{V} \langle \delta V^2 \rangle_{NPT},$$

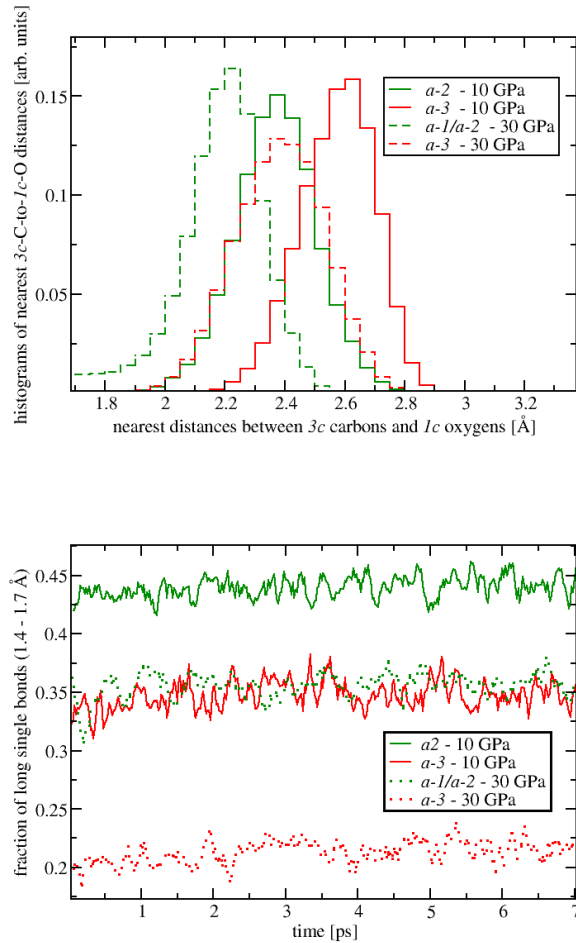


FIG. 7: (Color online) (a) Histograms of nearest distances between 3c carbons and 1c oxygens for polymeric *a*-carbonia *a-2* (green histogram) at 10 GPa and intermediate state *a-1/a-2* (dashed green) at 30 GPa and *a-3* at 10 GPa (red) and at 30 GPa (red dashed), all at 500 K. The histograms are scaled to the total number of 3c carbons in the system. (b) Fraction of C-O single bonds with length between 1.4 and 1.7 Å calculated for each frame during a 7 ps time interval extracted from the MD runs and scaled to total numbers of C-O single bonds. Colors and line styles represent the same systems and conditions as in (a) - systems at 30 GPa are marked with dotted lines. Full lines and dashed/dotted lines are to be compared separately as different line styles represent different simulation pressures and line colors distinct between polymeric and *a-3* form.

where V is average volume.

All calculated values of B were extracted from separate MD trajectories at 200 K lasting 40-60 ps to assure converged values of $\langle \delta V^2 \rangle_{NPT}$. From Table I we see that upon progressive transformation from *a-1* to molecular states the value of B decreases by more than an order of magnitude. The *molecular amorphous* corresponds to 200 K quenched molecular amorphous state (glass) ob-

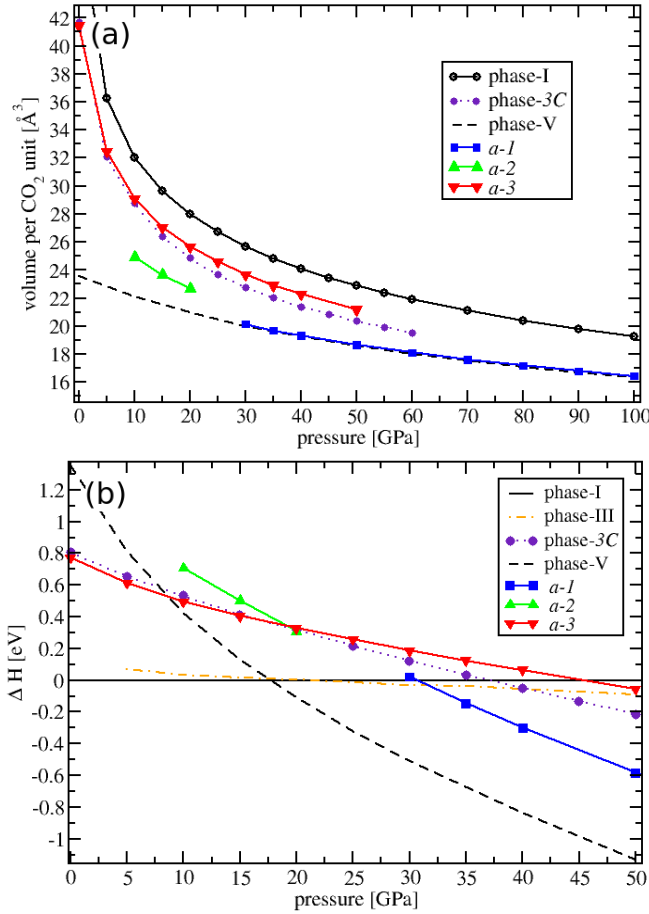


FIG. 8: (Color online) (a) Equation of states for $V(P)$ - volume per CO₂ unit versus pressure of phase-I (line with empty circles), phase-V (dashed line), phase-3C (violet dotted line with circles) and amorphous $a-1$ (blue squares), $a-2$ (green up triangles) and $a-3$ (red down triangles) in 1 Mbar range. (b) Enthalpies from 0 to 50 GPa relative to phase-I (horizontal line) per CO₂ unit of crystalline phase-III (orange dashed-dotted line), phase-3C (violet dotted line with circles), phase-V (black dashed line) and amorphous $a-1$ (blue squares), $a-2$ (green up triangles) and $a-3$ (red down triangles). All phase curves are shown only in their stability regions, where they survived optimization.

tained from molecular gas that appeared at the end of the original 500 K decompression (see Fig. 1).

We also calculated electronic properties of the amorphous forms within the PBE approximation and found that $a-3$ is an insulator with energy bandgap 3.35 eV at 5 GPa and $a-2$ is a semiconductor with 1.71 eV bandgap at 20 GPa. In $a-1$ at 40 GPa, the gap energy is decreased to 1.48 eV, while at 90 GPa it narrows to 0.7 eV. Therefore, polymerization into a tetrahedral-like amorphous form is not followed by metalization, though closure of the bandgap can be expected at Mbar conditions²⁴. We remark that the predicted LLT in CO₂ is also not accom-

Phase	bulk B [GPa]	P [GPa]
phase-V	294	40
$a-1$	282	40
$a-2$	75	5
$a-3$	46	0
phase-I	25	0
molecular amorphous	20	0

TABLE I: Calculated values of B at 200 K from hardest phase-V to soft molecular phases. B of phase-V at 40 GPa is reaching 300 GPa corresponding very well with theoretical predictions - Dong *et al.*^{58,75} and actual recent experimental measurements - Datchi *et al.*⁵².

panied by metalization²², which was noted to be exceptional for a molecular-polymeric transition in a high- T liquid state.

In order to present quantities directly comparable to experiments, we calculated static structure factors $S(Q)$ of the amorphous forms - Fig. 9. $S(Q)$ functions were calculated from the MD trajectories by the method described in Refs.^{76,77}. We first calculated $S(\vec{Q}_{hkl})$ at discrete set of \vec{Q}_{hkl} vectors (determined by the periodic boundary conditions) and then made convolution with Gaussian of width 0.1 Å⁻¹ to obtain $S(Q)$. This quantity was afterwards averaged over the corresponding trajectory. The normalization of the structure factors was chosen according to Ref.¹⁹ (and the Supplemental Material therein), where $S(Q)$ was factorized to the molecular formfactor $(f_C(Q) + 2f_O(Q))^2$, where $f_C(Q)$ and $f_O(Q)$ are atomic formfactors of carbon and oxygen, respectively. The calculated structure factors can then be directly compared to the experimental ones on Figure 4 of Ref.¹⁹.

The experimental curve at 41 GPa appears similarly to our curve of $a-1$ at 40 GPa - both contain main first peak at around 3.3 Å⁻¹. Upon decompression, our peak progressively shifts to lower Q values - $a-2$ and becomes broader when molecules are created - $a-3$. Finally, upon transition to the molecular state (in the glass), the peak appears to become split which is similar to the experimental data at 12 GPa, when a-carbonia was already transformed into the molecular amorphous form. This indicates that our simulated forms of a-carbonia could be associated with the earlier experimental observations¹⁹.

IV. CONCLUSIONS

Using ab initio MD simulations we performed decompression of polymeric a-carbonia initially prepared at high-pressure and observed several amorphous forms which behaved like mechanically stable and long-living metastable states. As the pressure decreases the original high-pressure polymeric form ($a-1$) with mostly four-coordinated carbon atoms and tetrahedral geometry first gradually transforms into less dense structures eventually

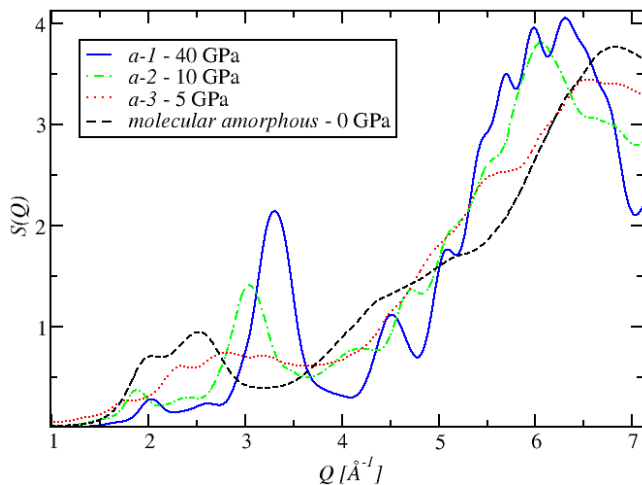


FIG. 9: (Color online) Static structure factors of *a-1* (blue line) at 40 GPa, *a-2* (green dashed-dotted line) at 10 GPa, *a-3* (red dotted) at 5 GPa and *molecular amorphous* form - glass (dashed black) at 0 GPa. The structural evolution from *a-1* to *a-2*, *a-3* and to *molecular amorphous* form is represented mainly by broadening and shifting of the first main $S(Q)$ peak to lower Q - from 3.3 \AA^{-1} in *a-1* to 2.5 \AA^{-1} in the molecular state.

reaching a limiting form (*a-2*) with roughly equal number of four and three-coordinated carbons. Both these forms were observed in the earlier simulations^{27,29,61}. Upon further decompression molecules start to appear and a new mixed molecular-polymeric form (*a-3*) is found before the system finally transforms to a fully molecular state. In the mixed form four-coordinated carbon atoms act as nodes that are connected by chains of three-coordinated carbons, while space between the chains is filled with

molecules. Compared to the polymeric forms the mixed *a-3* form appears to have pronounced metastability which can be related to different distribution of certain interatomic distances and bond lengths. Due to the large gap between the timescale of experiments and simulations it is not trivial to extrapolate the metastability observed in our simulations to true metastability at experimental conditions. However, the facts that the two polymeric forms were also reported in previous simulations and that the mixed molecular-polymeric form was prepared in our simulations in two independent pathways suggest that these states might indeed represent observable amorphous phases. We believe that it would be interesting to experimentally verify our predictions by carefully monitoring the structural evolution in a-CO_2 in a slow gradual decompression performed at low temperature, where the kinetics is slower.

Acknowledgments

This work was supported by the Slovak Research and Development Agency under Contract No. APVV-0558-10 and No. APVV-0733-11 and by the project implementation 26220220004 within the Research & Development Operational Programme funded by the ERDF. Part of the calculations were performed in the Computing Centre of the Slovak Academy of Sciences using the supercomputing infrastructure acquired in project ITMS 26230120002 and 26210120002 (Slovak infrastructure for high-performance computing) supported by the Research & Development Operational Programme funded by the ERDF.

-
- * Electronic address: plasienska@fmph.uniba.sk
- ¹ S. M. Sharma and S. K. Sikka, Prog. Mat. Sci. **40**, 1 (1996).
 - ² P. F. McMillan, J. Mater. Chem. **14**, 1506 (2004).
 - ³ M. C. Wilding, M. Wilson, and P. F. McMillan, Chem. Soc. Rev. **35**, 964986 (2006).
 - ⁴ J. P. Itié, A. Polian, G. Calas, J. Petiau, A. Fontaine, and H. Tolentino, Phys. Rev. Lett. **63**, 398 (1989).
 - ⁵ M. Guthrie, C. A. Tulk, C. J. Benmore, J. Xu, J. L. Yarger, D. D. Klug, J. S. Tse, H.-K. Mao, and R. J. Hemley, Phys. Rev. Lett. **93**, 115502 (2004).
 - ⁶ X. Hong, G. Shen, V. B. Prakapenka, M. Newville, M. L. Rivers, and S. R. Sutton, Phys. Rev. B **75**, 104201 (2007).
 - ⁷ G. Lelong, L. Cormier, G. Ferlat, V. Giordano, G. S. Henderson, A. Shukla, , and G. Calas, Phys. Rev. B **85**, 134202 (2012).
 - ⁸ S. K. Deb, M. Wilding, M. Somayazulu, and P. F. McMillan, Nature **414**, 528 (2001).
 - ⁹ E. Principi, A. DiCiccio, F. Decremps, A. Polian, S. DePanfilis, and A. Filipponi, Phys. Rev. B **69**, 201201 (2004).
 - ¹⁰ C. Sanloup, E. Gregoryanz, O. Degtyareva, and M. Hanfland, Phys. Rev. Lett. **100**, 075701 (2008).
 - ¹¹ Y. Lin, L. Zhang, H. K. Mao, P. Chow, Y. Xiao, M. Baldini, J. Shu, and W. L. Mao, Phys. Rev. Lett. **107**, 175504 (2011).
 - ¹² Y. Katayama, T. Mizutani, W. Utsumi, O. Shimomura, M. Yamakata, and K. ichi Funakoshi, Nature **403**, 170 (2000).
 - ¹³ R. Bellissent, L. Descotes, F. Boué, and P. Pfeuty, Phys. Rev. B **41**, 2135 (1990).
 - ¹⁴ G. D. Mukherjee and R. Boehler, Phys. Rev. Lett. **99**, 225701 (2007).
 - ¹⁵ A. F. Goncharov, J. C. Crowhurst, V. V. Struzhkin, and R. J. Hemley, Phys. Rev. Lett. **101**, 095502 (2008).
 - ¹⁶ B. Boates and S. A. Bonev, Phys. Rev. Lett. **102**, 015701 (2009).
 - ¹⁷ J. N. Glosli and F. H. Ree, Phys. Rev. Lett. **82**, 4659 (1999).
 - ¹⁸ S. Scandolo, Proc. Nat. Acad. Sci. **124**, 244704 (2006).
 - ¹⁹ M. Santoro, F. A. Gorelli, R. Bini, G. Ruocco, S. Scandolo, and W. A. Crichton, Nature **441**, 857 (2006).
 - ²⁰ T. Kume, Y. Ohya, M. Nagata, S. Sasaki, and H. Shimizu, Jour. Appl. Phys. **102**, 53501 (2007).

- ²¹ B. Boates, S. Hamel, E. Schwegler, and S. A. Bonev, J. Chem. Phys. **134**, 064504 (2011).
- ²² B. Boates, A. M. Teweldeberhan, and S. A. Bonev, Proc. Nat. Acad. Sci. **109**, 1480814812 (2012).
- ²³ M. Santoro and F. A. Gorelli, Chem. Soc. Rev. **35**, 918 (2006).
- ²⁴ C.-S. Yoo, Phys. Chem. Chem. Phys. **15**, 7949 (2013).
- ²⁵ A. R. Oganov, R. J. Hemley, R. M. Hazen, and A. P. Jones, Reviews in Mineralogy & Geochemistry **75**, 47 (2013).
- ²⁶ V. Iota, C.-S. Yoo, J.-H. Klepeis, Z. Jenei, W. Evans, and H. Cynn, Nature Materials **6**, 34 (2007).
- ²⁷ J. A. Montoya, R. Rousseau, M. Santoro, F. Gorelli, and S. Scandolo, Phys. Rev. Lett. **100**, 163002 (2008).
- ²⁸ M.-S. Lee, J. A. Montoya, and S. Scandolo, Phys. Rev. B **79**, 144102 (2009).
- ²⁹ J. Sun, D. D. Klug, R. Martoňák, J. A. Montoya, M.-S. Lee, S. Scandolo, and E. Tosatti, PNAS **106**, 6077 (2009).
- ³⁰ A. Togo, F. Oba, and I. Tanaka, Phys. Rev. B **77**, 184101 (2008).
- ³¹ C.-S. Yoo, H. Cynn, F. Gygi, G. Galli, V. Iota, M. Nicol, S. Carlson, D. Häusermann, and C. Mailhot, Phys. Rev. Lett. **83**, 5527 (1999).
- ³² C.-S. Yoo, H. Kohlmann, H. Cynn, M. F. Nicol, V. Iota, and T. LeBihan, Phys. Rev. B **65**, 104103 (2002).
- ³³ V. Iota and C.-S. Yoo, Phys. Rev. Lett. **86**, 5922 (2001).
- ³⁴ C.-S. Yoo, V. Iota, and H. Cynn, Phys. Rev. Lett. **86**, 444 (2001).
- ³⁵ J.-H. Park, C. S. Yoo, V. Iota, H. Cynn, M. F. Nicol, and T. LeBihan, Phys. Rev. B **68**, 014107 (2003).
- ³⁶ F. Datchi, V. M. Giordano, P. Munsch, and A. M. Saitta, Phys. Rev. Lett. **103**, 185701 (2009).
- ³⁷ F. A. Gorelli, V. M. Giordano, P. R. Salvi, and R. Bini, Phys. Rev. Lett. **93**, 205503 (2004).
- ³⁸ B. Holm, R. Ahuja, A. Belonoshko, and B. Johansson, Phys. Rev. Lett. **85**, 1258 (2000).
- ³⁹ S. A. Bonev, F. Gygi, T. Ogitsu, and G. Galli, Phys. Rev. Lett. **91**, 065501 (2003).
- ⁴⁰ H. Olijnyk and A. P. Jephcoat, Phys. Rev. B **57**, 879 (1998).
- ⁴¹ C.-S. Yoo, A. Sengupta, and M. Kim, High Press. Res. **31**, 6874 (2011).
- ⁴² O. Tschauer, H.-K. Mao, and R. J. Hemley, Phys. Rev. Lett. **87**, 075701 (2001).
- ⁴³ A. R. Oganov, S. Ono, Y. Ma, C. W. Glass, and A. Garcia, Earth Planet. Sci. Lett. **273**, 38 (2008).
- ⁴⁴ K. D. Litasov, A. F. Goncharov, and R. J. Hemley, Earth Planet. Sci. Lett. **309**, 318 (2011).
- ⁴⁵ Y. Seto, D. Hamane, T. Nagai, and K. Fujino, Phys. Chem. Minerals **35**, 223229 (2008).
- ⁴⁶ N. Takafuji, K. Fujino, T. Nagai, Y. Seto, and D. Hamane, Phys. Chem. Minerals **33**, 651654 (2006).
- ⁴⁷ C.-S. Yoo, A. Sengupta, and M. Kim, Angew. Chem. Int. Ed. **50**, 11219 (2011).
- ⁴⁸ A. M. Teweldeberhan, B. Boates, and S. Bonev, Earth Planet. Sci. Lett. **373**, 228232 (2013).
- ⁴⁹ K. Aoki, H. Yamawaki, M. Sakashita, Y. Gotoh, and K. Takemura, Science **263**, 356 (1994).
- ⁵⁰ B. Kuchta and R. D. Etters, Phys. Rev. B **47**, 14691 (1993).
- ⁵¹ V. Iota, C.-S. Yoo, and H. Cynn, Science **283**, 1510 (1999).
- ⁵² F. Datchi, B. Mallick, A. Salamat, and S. Ninet, Phys. Rev. Lett. **108**, 125701 (2012).
- ⁵³ M. Santoro, F. A. Gorelli, R. Bini, J. Haines, O. Cambone, C. Levelut, J. A. Montoya, and S. Scandolo, PNAS **109**, 5176 (2012).
- ⁵⁴ C.-S. Yoo, M. Kim, W. Morgenroth, and P. Liermann, Phys. Rev. B **87**, 214103 (2013).
- ⁵⁵ V. M. Giordano and F. Datchi, Europhys. Lett. **77**, 46002 (2007).
- ⁵⁶ A. Sengupta and C.-S. Yoo, Phys. Rev. B **80**, 014118 (2009).
- ⁵⁷ A. Sengupta and C.-S. Yoo, Phys. Rev. B **82**, 012105 (2010).
- ⁵⁸ J. Dong, J. K. Tomfohr, and O. F. Sankey, Phys. Rev. B **61**, 5967 (2000).
- ⁵⁹ A. Sengupta, M. Kim, C.-S. Yoo, and J. S. Tse, J. Phys. Chem. C **116**, 2061 (2012).
- ⁶⁰ M. Santoro and F. A. Gorelli, Phys. Rev. B **80**, 184109 (2009).
- ⁶¹ S. Serra, C. Cavazzoni, G. L. Chiarotti, S. Scandolo, and E. Tosatti, Science **284**, 788 (1999).
- ⁶² M. Santoro, J.-F. Lin, H.-K. Mao, and R. J. Hemley, Jour. Chem. Phys. **121**, 2780 (2004).
- ⁶³ G. Kresse and J. Furthmüller, Phys. Rev. B **54**, 11169 (1996).
- ⁶⁴ G. Kresse and J. Furthmüller, Comput. Mat. Sci. **6**, 15 (1996).
- ⁶⁵ H. J. C. Berendsen, J. P. M. Postma, W. F. van Gunsteren, A. DiNola, and J. R. Haak, J. Chem. Phys. **81**, 3684 (1984).
- ⁶⁶ D. Plašienka and R. Martoňák, Phys. Rev. B **85**, 094112 (2012).
- ⁶⁷ M. Parrinello and A. Rahman, Phys. Rev. Lett. **45**, 1196 (1980).
- ⁶⁸ J. P. Perdew, K. Burke, and M. Ernzerhof, Phys. Rev. Lett. **77**, 3865 (1996).
- ⁶⁹ Jmol: an open-source java viewer for chemical structures in 3d. <http://www.jmol.org/>.
- ⁷⁰ J. Peralta, G. Gutiérrez, and J. Rogan, J. Phys.: Condens. Matter **20**, 145215 (2008).
- ⁷¹ E. Lewars, Theo. Chem. **363**, 1 (1995).
- ⁷² G. Frapper and J.-Y. Saillard, J. Am. Chem. Soc. **122**, 5367 (2000).
- ⁷³ F. Tassone, G. L. Chiarotti, R. Rousseau, S. Scandolo, and E. Tosatti, Chem. Phys. Chem. **6**, 1752 (2005).
- ⁷⁴ M. P. Allen and D. J. Tildesley, *Computer Simulation of Liquids* (Oxford University Press, 1987), ISBN 0-19-855375-7.
- ⁷⁵ J. Dong, J. K. Tomfohr, O. F. Sankey, K. Leinenweber, M. Somayazulu, and P. F. McMillan, Phys. Rev. B **62**, 14685 (2000).
- ⁷⁶ J. M. Holender and G. J. Morgan, J. Phys.: Condens. Matter **3**, 1947 (1991).
- ⁷⁷ Y. Liang, Ph.D. thesis, International School for Advanced Studies (SISSA) (2007).
- ⁷⁸ Simulations of initial compression and 500 K branch decompression were performed with VASP 4 and Berendsen barostat, while lower-*T* branch decompression and all other calculations were calculated with VASP 5 and PR barostat.
- ⁷⁹ In the experiments, nanocrystalline and amorphous phases also cannot be always distinguished due to finite resolution ability of the device.
- ⁸⁰ C-O type RDF of *a*-3 shows two distinct nearest peaks corresponding to two different C=O double bonds present in it - shorter 1.17 Å in CO₂ molecules and longer 1.18 Å coming from double bonds on 3c carbons.